# Symmorphic linked nodal rings in semiconducting layers

Cheng Gong[1], Yuee Xie[1], Yuanping Chen[1]*, Heung-sik Kim[2] and David Vanderbilt[2]

[1]*School of Physics and Optoelectronics, Xiangtan University, Xiangtan, 411105, Hunan, China*
[2]*Department of Physics and Astronomy, Rutgers University, Piscataway, New Jersey 08854-8019, USA*

The unique properties of topological semimetals have strongly driven efforts to seek for new topological phases and related materials. Here, we identify a critical condition for the existence of linked nodal rings (LNRs) in symmorphic crystals, and propose that three types of LNRs, named as α-, β- and γ-type, can be obtained by stacking semiconducting layers. Several honeycomb structures are suggested to be topological LNR semimetals, including layered and "hidden" layered structures. Transitions between the three types of LNRs can be driven by external strains. Interesting surface states other than drumhead states are found in these topological materials.

Corresponding author: chenyp@xtu.edu.cn

Following the experimental detection of Fermi-arc surface states in Weyl semimetals[1-3], considerable attention has focused on the investigation of topological semimetals/metals (TMs) more generally[4-8]. Classic examples of TMs are the Weyl and Dirac semimetals[9-15], which exhibit twofold and fourfold degenerate Fermi points respectively. These nodal-point semimetals display a number of exotic transport phenomena such as negative magnetoresistance and the chiral magnetic effect[16-19]. Nodal line/ring semimetals belong to another class of TMs[20-26], in which the valence and conduction bands cross along one-dimensional lines in three-dimensional k-space. In general, the line is not pinned at the Fermi energy[27-29], but passes through the Fermi energy at discrete points. As a consequence, the Fermi surface takes the shape of a thin tube with changing radius, possibly with constrictions. These semimetals are expected to exhibit graphene-like Landau levels and enhanced sensitivity to long-range Coulomb interaction[30-35]. Unlike nodal points, nodal lines/rings can form various topologically connected structures such as chains[36,37], knots[38], and Hopf links[39-41], bringing new physics and topological properties.

On the other hand, two-dimensional materials are the focus of another recently thriving field[42]. After graphene, many graphene-like honeycomb structures have been proposed, and some of them have been fabricated successfully[43-48], including silicene, germanene, BN, and phosphorene. These not only show intrinsic interesting properties in single-sheet form, but also have interesting hybrid properties when stacked into three-dimensional (3D) materials[49-51]. These stacked structures often

have a mirror symmetry along the stacking direction, and since nodal lines/rings can be protected by mirror symmetry[52-55], it is natural to ask whether we can obtain topological nodal line/ring semimetals by the stacking of layered structures.

Here we identify a necessary condition for the existence of linked nodal lines in symmorphic crystal structures. By stacking semiconducting honeycomb layers, three types of linked nodal rings (LNRs), as shown in Fig. 1, are found to occur. The α-type consists of isolated crossed rings as in Panel (a), the β-type corresponds to a nodal chain like that in Panel (c), and the γ-type is the structure of ladder of parallel rings as in Panel (d). Moreover, the three topological phases can be converted into one another via application of external strain. Besides the drumhead states, interesting surface states, such as dumbbell states and annular states, are observed in the surface band structures of these LNR semimetals. Several 3D layered materials are suggested to possess the topological nodal rings, including BN, AlP, and GaP, and "hidden" layered structures SiC, BP, and BAs. A tight-binding (TB) model and a $k \cdot p$ model are used to explain the relations between the topological phases and how they evolve into one another.

For the LNRs to be protected, a critical necessary condition is *the presence of at least two intersecting mirror or glide planes commuting with each other* in the crystal structure[56]. For simplicity, here we consider only two bands (occupied/unoccupied) near the Fermi level in the presence of two mirror planes without spin-orbit coupling. Let us denote the two mirror planes in the momentum space as A and B, as shown in Fig. 1(a). The occupied and unoccupied bands on the AB-intersecting line, say

between points X and Y, can be labeled with two mirror eigenvalues $a^{\pm}$ and $b^{\pm}$ taking values ±1. The right half of Fig. 1(b) shows the bands on the XY-line. If the two bands have eigenvalue pairs $(a^{+},b^{+})$ and $(a^{-},b^{-})$ respectively, then they can cross without a gap opening[57]. If we deviate from the XY-line to look at the bands on a generic k-path residing in plane A (represented as a black curved arrow in Fig. 1(a)), then the two bands can cross again because of different A eigenvalues for each band, as depicted in the left half of Fig. 1(b). The same argument applies to plane B, hence this guarantees the presence of two nodal lines in planes A and B respectively, meeting at the band crossing point on the XY line and forming a nodal link. Note that non-symmorphic (glide or screws) characters are not mandatory, so this kind of nodal chains can exist even in symmorphic crystals[58,59,60], in contrast to a previous suggestion where the non-symmorphic nature was essential[36]. Whether the nodal lines are closed or open depends on details of the band dispersion, and the α-type LNR can be transformed into β- or γ-type as shown from our following results.

According to the necessary condition of LNRs, two structure types are considered (see Fig. 2). The first kind consists of 3D layered structures with $sp^2$-hybridization atoms, as shown in Fig. 1(a), with the planar layers stacked in an AA' stacking sequence. Each layer consists of hexagonal rings with each ring including two types of atoms labeled A1 and A2. The four-atom primitive cell (two A1 and two A2) is shown in Fig. 2(b). Atoms of the same type form dimers along the armchair direction, while those of opposite type make up the zigzag chains. The second structure type is a porous network in which $sp^2$-hybridized zigzag chains are

connected by $sp^3$-hybridized linker atoms (see Fig. 2(c). Its primitive cell in Fig. 2(d) includes six (two $sp^3$ and four $sp^2$) atoms. Since the bands closest to the Fermi level will be dominated by the $sp^2$ atoms, it is reasonable to neglect the $sp^3$-hybridized atoms in a first approximation, in which case the $sp^2$ atoms form a structure of buckled layers stacked in an AA' sequence. The angle θ between lattice vectors is defined in the figures. Both types of structures have two mirrors on the planes *xz* and *xy*.

Our first-principles calculations were based on the density functional theory (DFT) as implemented in the Vienna Ab-initio Simulation Package[61]. The core-valence interactions were described by projector augmented-wave (PAW) potentials within the Perdew-Burke-Ernzerhof (PBE) approximation for the exchange-correlation energy[62]. Plane waves with a kinetic energy cutoff of 500 eV were used as the basis set. We used the conjugate gradient method to optimize the atomic positions, and the energy convergence criterion between two consecutive steps was $10^{-5}$ eV. The maximum allowed force on the atoms is $10^{-3}$ eV/Å.

When only one orbital of each atom in Fig. 2(a) is considered, a 4×4 TB model can be used to describe its electronic properties:

$$H = \sum_i \varepsilon_\alpha a_i^\dagger a_i + \sum_{i,j} t_\beta a_i^\dagger a_j, \quad (1)$$

where $a_i^\dagger / a_j$ represent the creation/annihilation operators, $\varepsilon_\alpha$ $(\alpha = 1,2)$ represent site energies of atoms A1 and A2, $t_\beta$ $(\beta = 1 \ldots 7)$ are the hopping parameters between atoms. Here $t_1$ to $t_5$ describe the intra-layer interactions, while $t_6$ and $t_7$ describe the inter-layer couplings [see Fig. 2(b)]. When the $sp^3$-hybridization atoms in

Fig. 2(c) are neglected, the porous network becomes a layered structure. From this point of view, the main difference between the structures of Figs. 2(a) and 2(c) is that the layers in the latter are buckled rather than planar. Because of this close analogy, Eq. (1) can be used to describe the electronic properties of both structures.

We start from a semiconducting single layer. In this case the interlayer interactions in Eq. (1) can be omitted, i.e., we can set $t_6 = t_7 = 0$. The dashed red lines in Fig. 3(a) show the band structure of a typical single-layer semiconductor. It has a substantial band gap, and completely flat bands along paths Z-T, R-T and T-S because of the absence of interlayer couplings. When the semiconducting layers are stacked into a 3D structure, the interlayer couplings $t_6$ and $t_7$ become involved. As a result, the flat bands become dispersive (solid blue lines), and the conduction and valence bands cross at the Fermi level. In Fig. 3(a) these crossings look like Dirac points, but as we shall see, they link together in 3D to form nodal rings or lines.

By tuning the parameters in Eq. (1), the three types of LNRs in Fig. 1 can be generated. Figure 3(a) presents the band structure for the α-type rings. One can find that there are crossings along Z-T, T-Y, R-T and T-C. In the full BZ, these crossing points lie on two perpendicular nodal rings with a common center at T, as shown in Fig. 3(d). One ring lies on the $k_a = k_b$ plane (plane A) while the other lies on the $k_c = 0$ plane (plane B); the crossing point is denoted as H. By comparing the band eigenvalues, it can be seen that this pattern corresponds to the α-type phase in Fig. 1(a).

By increasing the intralayer hoppings while decreasing the interlayer ones, the

band structure in Fig. 3(a) evolves into that of Fig. 3(b) by inverting occupied/unoccupied bands at C and R points, after which we find crossings along Z-T, T-Y and C-Z. These crossing points lie on two perpendicular LNRs on planes $k_a$ = $k_b$ and $k_c$ = 0 centered on the points T and Z respectively, as shown in Fig. 3(e). They link in the full BZ and form a nodal chain, corresponding to the β-type phase in Fig. 1(c). This phase is different from the type of nodal chain described in Ref. [36], which is protected by a nonsymmorphic glide-plane symmetry.

By contrast, when the intralayer hoppings are decreased while the interlayer ones are increased, the band structure in Fig. 3(a) evolves into that of Fig. 3(c) by inducing a band inversion at Z. This introduces an additional nodal ring on the A plane encircling Z, and the ring on the B plane is now open and connects the two rings on plane A as shown in Fig. 3(f). The crossing points are now located on the k paths Γ-Z, T-Y, R-T, T-C and C-Z. In the extended BZ the nodal structure has an appearance like a ladder of parallel rings, corresponding to the γ-type phase in Fig. 1(d). The topological protection of the three types of LNRs can also be inferred from their 1D winding numbers along a close path $\mathcal{L}$ encircling the rings: $N_{\mathcal{L}} = \frac{1}{\pi}\oint_{\mathcal{L}} d\boldsymbol{k} \cdot A(\boldsymbol{k})$, where $A(\boldsymbol{k})$ is the Berry connection at the point $\boldsymbol{k}$. The calculation results indicate that all of them have nontrivial values.

Comparing the four-band TB model in Eq. (1), we can construct a two-band k · p model to further compare the LNRs. All the three types of LNRs have a common nodal ring centered on the point T (see Figs. 3(d-f)). Constrained by the symmetries and the time reversal symmetry for a spinless system, one obtains a model

up to quadratic order in *k* around T as

$$H(q_x, q_y, q_z) = \begin{pmatrix} A_1 q_x^2 + B_1 q_y^2 + C_1 q_z^2 & -iDq_x q_y \\ iDq_x q_y & \Delta + A_2 q_x^2 + B_2 q_y^2 + C_2 q_z^2 \end{pmatrix} \quad (2)$$

where $q_i = k_i - k_{i0}$ ($i$ = $x$, $y$, $z$) and $(k_{x0}, k_{y0}, k_{z0})$ is the momentum coordinate at point T. The parameters $\Delta$, $A_1$, $B_1$, $C_1$, $A_2$, $B_2$, $C_2$, and $D$ are determined by fitting DFT or TB results. When $A_1$, $B_1$, $C_1$ >0 and $A_2$, $B_2$, $C_2$ <0, it produces a α-type phase; when $A_1$, $B_2$, $C_1$ > 0 and $A_2$, $B_1$ $C_2$ <0, a β-type-like phase is produced, in which a nodal ring linked two curved nodal lines; when $A_1$, $C_1$ >0, $A_2$, $C_2$ <0 and $B_1$, $B_2$ = 0, a γ-type-like phase is produced, where a nodal ring linked two straight nodal lines.

To find topological materials possessing the three LNR phases, we construct structures like Figs. 2(a) and 2(c) based on IV or III/V elements. By calculating band structures, we find that layered structures BN, AlP and GaP and "hidden" layered structures SiC, BP and BAs can fit the requirements (see Fig. S1 in SI). The structural parameters of these structures are shown in Table S1. We calculate their phonon dispersions, and find that there are no soft modes in the spectra of BN and SiC (see Fig. S2 in SI). This indicates that BN and SiC are metastable structures having good stability. Therefore, BN and SiC are used as two examples to exhibit the topological properties.

Figure 4(a) shows the band structure of single-layer honeycomb BN, which we find to be a semiconductor with a direct band gap. After the BN layers are stacked into 3D structure by AA' stacking, the band structure changes as shown in Fig. 4(b), which looks quite similar to Fig. 3(a). A close examination indicates that there are

indeed α-type nodal rings in BZ. The projections of the band structures illustrate that the states around the Fermi level are contributed mainly by $p_z$ orbitals on B and N atoms. Therefore, it is reasonable that we use Eq. (1) to describe the structures.

The band structure of "hidden" layered SiC structure is shown in Fig. 4(c). It is also very similar to the spectrum in Fig. 3(a), and α-type nodal rings are also found here. As mentioned above, the α-type phase evolves into β- and γ-type phases by tuning the intra- and interlayer hopping energies. An external strain along the direction (110) can induce the same effect as the variation of hopping parameters. As the angle θ changes with the strain from 89º to 80º, meanwhile He atoms are squeezed into the holes of the porous structure (see the inset in Fig. 4(d)), the band structure changes to that of Fig. 4(d). It is similar to the band spectrum in Fig. 3(c), which means that the system is changed to a β-type nodal-ring semimetal. After θ is increased further from 89º to 108º, the band structure in Fig. 4(e) corresponds to the γ-type nodal rings. As seen from Figs. 4(c-e), all three types of LNR structures are accessible for SiC under strain.

Figure 5 presents the surface band structures of the three kinds of LNRs, in which Figs. 5(a-c) and 5(d-f) correspond to the [010] and $[\bar{1}10]$ surfaces respectively. On the [010] surface, we find that all types of LNRs exhibit drumhead states inside the projections of the nodal rings, while the surface states on the $[\bar{1}10]$ surface are different. The surface states of the α-type phase are still drumhead states, as shown in Fig. 5(d). Instead, in the cases of β- and γ-type nodal rings, the linking of the nodal rings induces exotic surface states. In Fig. 5(e), the surface states are distributed in a

dumbbell-like region with the two ends corresponding to overlap regions. In Fig. 5(f), the surface state region has the appearance of a donut or an annular eclipse, because the projection of one ring is right in the center of the other. The areas of the surface state regions can be tuned by strain, and the transition between the three types of linked rings can also be tuned.

In conclusion, we propose three types of LNRs showing distinct topological surface states, and an essential condition for the presence of them. Our results suggest a guiding principle to engineer LNR semimetals; preserving two mirror and/or glide symmetries intersecting and commuting with each other and applying strain or pressure. We comment that this idea is a generic one and not system-specific. Also, it should be helpful in realizing LNR not only in fermionic systems but also in photonics crystals or other bosonic lattices, shedding light on nodal line engineering for further studies.

YPC and YEX were supported by the National Natural Science Foundation of China (Nos. 51376005 and 11474243). DV was supported by NSF DMR-1408838 and HSK was supported by NSF DMREF DMR-1629059.

# Reference


[1] B. Lv *et al.*, Phys. Rev. X **5**, 031013 (2015).
[2] S. Y. Xu *et al.*, Science **347**, 294 (2015).
[3] S.-Y. Xu *et al.*, Science **349**, 613 (2015).
[4] Q. L. He *et al.*, Science **357**, 294 (2017).
[5] H. Huang, S. Zhou, and W. Duan, Phys. Rev. B **94**, 121117 (2016).
[6] L. Lu, Z. Wang, D. Ye, L. Ran, L. Fu, J. D. Joannopoulos, and M. Soljačić, Science **349**, 622 (2015).
[7] B. Q. Lv *et al.*, Nature (London) **546**, 627 (2017).
[8] A. A. Soluyanov, D. Gresch, Z. Wang, Q. Wu, M. Troyer, X. Dai, and B. A. Bernevig, Nature (London) **527**, 495 (2015).
[9] X. Wan, A. M. Turner, A. Vishwanath, and S. Y. Savrasov, Phys. Rev. B **83**, 205101 (2011).
[10] Z. Wang, Y. Sun, X.-Q. Chen, C. Franchini, G. Xu, H. Weng, X. Dai, and Z. Fang, Phys. Rev. B **85**, 195320 (2012).
[11] Z. Liu *et al.*, Science **343**, 864 (2014).
[12] Z. K. Liu *et al.*, Nat. Mater. **13**, 677 (2014).
[13] Y. Chen, Y. Xie, S. A. Yang, H. Pan, F. Zhang, M. L. Cohen, and S. Zhang, Nano Lett. **15**, 6974 (2015).
[14] H. Weng, C. Fang, Z. Fang, B. A. Bernevig, and X. Dai, Phys. Rev. X **5**, 011029 (2015).
[15] C. Zhong, Y. Chen, Z. M. Yu, Y. Xie, H. Wang, S. A. Yang, and S. Zhang, Nat. Commun. **8**, 15641 (2017).
[16] D. Son and B. Spivak, Phys. Rev. B **88**, 104412 (2013).
[17] X. Huang *et al.*, Phys. Rev. X **5**, 031023 (2015).
[18] F. Arnold *et al.*, Nat. Commun. **7**, 11615 (2016).
[19] H. Li, H. He, H. Z. Lu, H. Zhang, H. Liu, R. Ma, Z. Fan, S. Q. Shen, and J. Wang, Nat. Commun. **7**, 10301 (2016).
[20] A. Burkov, M. Hook, and L. Balents, Phys. Rev. B **84**, 235126 (2011).
[21] L. Lu, L. Fu, J. D. Joannopoulos, and M. Soljačić, Nat. Photon. **7**, 294 (2013).
[22] C. Fang, Y. Chen, H.-Y. Kee, and L. Fu, Phys. Rev. B **92**, 081201 (2015).
[23] Y. Kim, B. J. Wieder, C. L. Kane, and A. M. Rappe, Phys. Rev. Lett. **115**, 036806 (2015).
[24] R. Yu, H. Weng, Z. Fang, X. Dai, and X. Hu, Phys. Rev. Lett. **115**, 036807 (2015).
[25] H. Huang, J. Liu, D. Vanderbilt, and W. Duan, Phys. Rev. B **93**, 201114 (2016).
[26] J. T. Wang, H. Weng, S. Nie, Z. Fang, Y. Kawazoe, and C. Chen, Phys. Rev. Lett. **116**, 195501 (2016).
[27] G. Xu, H. Weng, Z. Wang, X. Dai, and Z. Fang, Phys. Rev. Lett. **107**, 186806 (2011).
[28] L. M. Schoop *et al.*, Nat. Commun. **7**, 11696 (2016).
[29] Q. Xu, R. Yu, Z. Fang, X. Dai, and H. Weng, Phys. Rev. B **95**, 045136 (2017).
[30] J. González, F. Guinea, and M. Vozmediano, Phys. Rev. Lett. **77**, 3589 (1996).
[31] V. N. Kotov, B. Uchoa, V. M. Pereira, F. Guinea, and A. H. Castro Neto, Rev. Mod. Phys. **84**, 1067 (2012).

[32] S.-K. Jian and H. Yao, Phys. Rev. B **92**, 045121 (2015).
[33] H.-H. Lai, Phys. Rev. B **91**, 235131 (2015).
[34] J.-W. Rhim and Y. B. Kim, Phys. Rev. B **92**, 045126 (2015).
[35] Y. Huh, E.-G. Moon, and Y. B. Kim, Phys. Rev. B **93**, 035138 (2016).
[36] T. Bzdusek, Q. Wu, A. Ruegg, M. Sigrist, and A. A. Soluyanov, Nature (London) **538**, 75 (2016).
[37] Z. Yan and Z. Wang, Phys. Rev. B **96**, 041206 (2017).
[38] M. Ezawa, Phys. Rev. B **96**, 041202 (2017).
[39] P.-Y. Chang and C.-H. Yee, arXiv:1704.01948.
[40] W. Chen, H.-Z. Lu, and J.-M. Hou, Phys. Rev. B **96**, 041102 (2017).
[41] Z. Yan, R. Bi, H. Shen, L. Lu, S.-C. Zhang, and Z. Wang, Phys. Rev. B **96**, 041103 (2017).
[42] K. S. Novoselov, A. K. Geim, S. V. Morozov, D. Jiang, Y. Zhang, S. V. Dubonos, I. V. Grigorieva, and A. A. Firsov, Science **306**, 666 (2004).
[43] M. E. Dávila, L. Xian, S. Cahangirov, A. Rubio, and G. Le Lay, New J. Phys. **16**, 095002 (2014).
[44] D. Hanlon *et al.*, Nat. Commun. **6**, 8563 (2015).
[45] G. Lu, T. Wu, Q. Yuan, H. Wang, H. Wang, F. Ding, X. Xie, and M. Jiang, Nat. Commun. **6**, 6160 (2015).
[46] P. Vogt, P. De Padova, C. Quaresima, J. Avila, E. Frantzeskakis, M. C. Asensio, A. Resta, B. Ealet, and G. Le Lay, Phys. Rev. Lett. **108**, 155501 (2012).
[47] J. L. Zhang *et al.*, Nano Lett. **16**, 4903 (2016).
[48] F. F. Zhu, W. J. Chen, Y. Xu, C. L. Gao, D. D. Guan, C. H. Liu, D. Qian, S. C. Zhang, and J. F. Jia, Nat. Mater. **14**, 1020 (2015).
[49] J. Hass, W. A. de Heer, and E. H. Conrad, J. Phys. Condens. Matter **20**, 323202 (2008).
[50] J. Qiao, X. Kong, Z. X. Hu, F. Yang, and W. Ji, Nat. Commun. **5**, 4475 (2014).
[51] Z. Zhu and D. Tomanek, Phys. Rev. Lett. **112**, 176802 (2014).
[52] G. Bian *et al.*, Nat. Commun. **7**, 10556 (2016).
[53] G. Bian *et al.*, Phys. Rev. B **93**, 121113 (2016).
[54] Y. H. Chan, C.-K. Chiu, M. Y. Chou, and A. P. Schnyder, Phys. Rev. B **93**, 205132 (2016).
[55] J. Zhao, R. Yu, H. Weng, and Z. Fang, Phys. Rev. B **94**, 195104 (2016).
[56] These considerations can also be generalized to non-symmorphic systems with intersecting glide and/or simple mirror planes. If these two operations anticommute with each other, however, a twofold degeneracy is enforced on the line instead of a band crossing at one point.
[57] A similar scenario applies to a crossing between bands ($a^+$,$b^-$) and ($a^-$,$b^+$).
[58] H. Weng, Y. Liang, Q. Xu, R. Yu, Z. Fang, X. Dai, and Y. Kawazoe, Phys. Rev. B **92**, 045108 (2015).
[59] T. Kawakami and X. Hu, arXiv:1611.07342.
[60] R. Yu, Q. Wu, Z. Fang, and H. Weng, arXiv:1701.08502.
[61] G. Kresse and J. Hafner, Phys. Rev. B **47**, 558 (1993).
[62] J. P. Perdew, K. Burke, and M. Ernzerhof, Phys. Rev. Lett. **77**, 3865 (1996).

## Figure captions

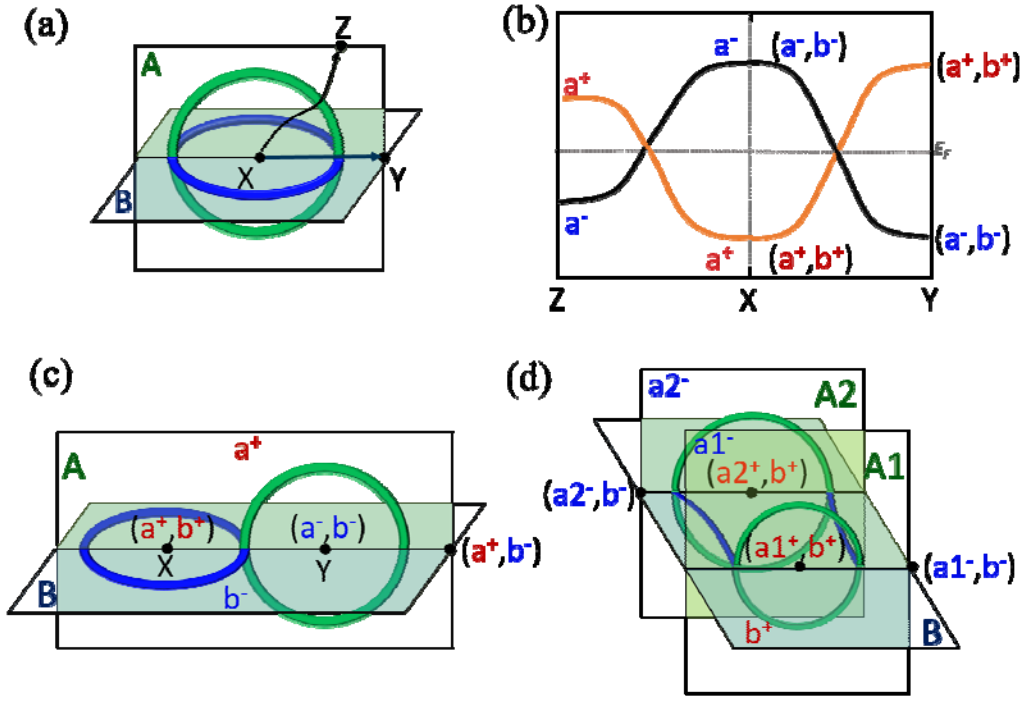


Figure 1. (color online) (a) An -type topological LNR, and (b) a simple model band structure manifesting nodal links from the two mirror symmetries A and B shown in (a). The right and left halves of (b) correspond to the bands on the k-path from points X to Y (straight arrow in (a)) and from X to Z (curved black arrows), respectively. Different color (red and blue) represents different symmetry eigenvalues. (c) -type and (d) -type topological LNRs. Symmetry eigenvalues of the occupied band are shown in (a), (c) and (d).

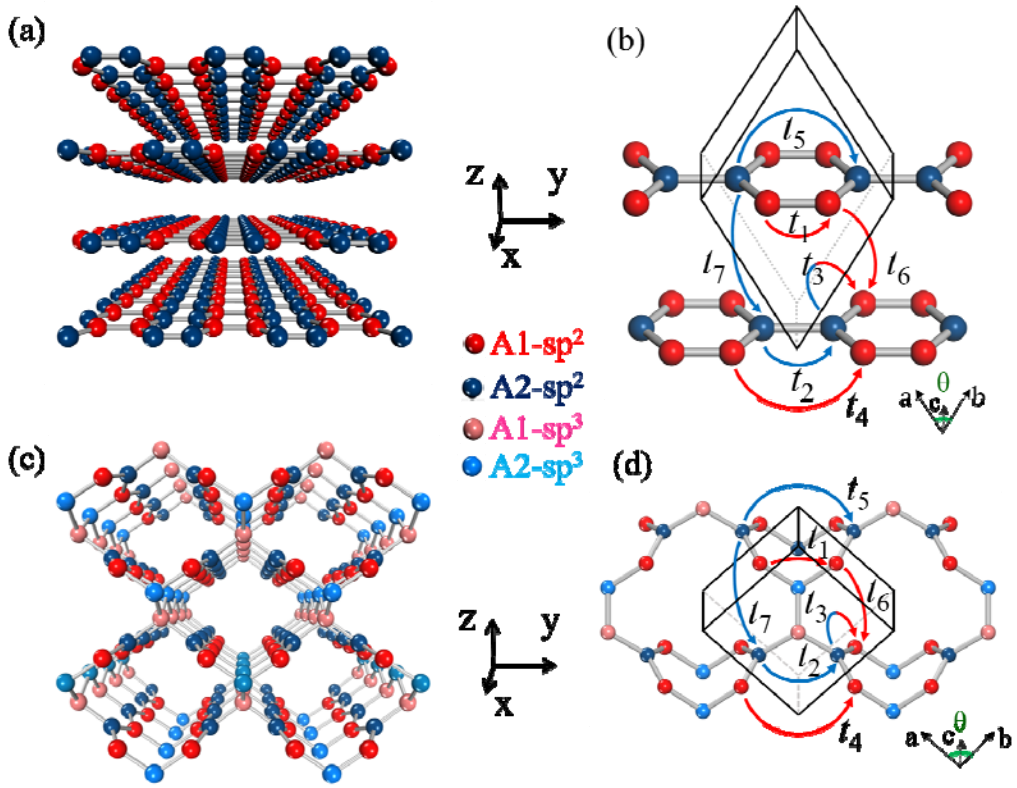


Figure 2. (color online) AA' stacked honeycomb layered structure (a) and its primitive cell (b). "Hidden" AA' stacked honeycomb layered network (c) and its primitive cell (d). Both of the structures are made of two kinds of atoms A1 and A2. $t_1$~$t_7$ in (b) and (d) describe the hopping parameters of the structures.

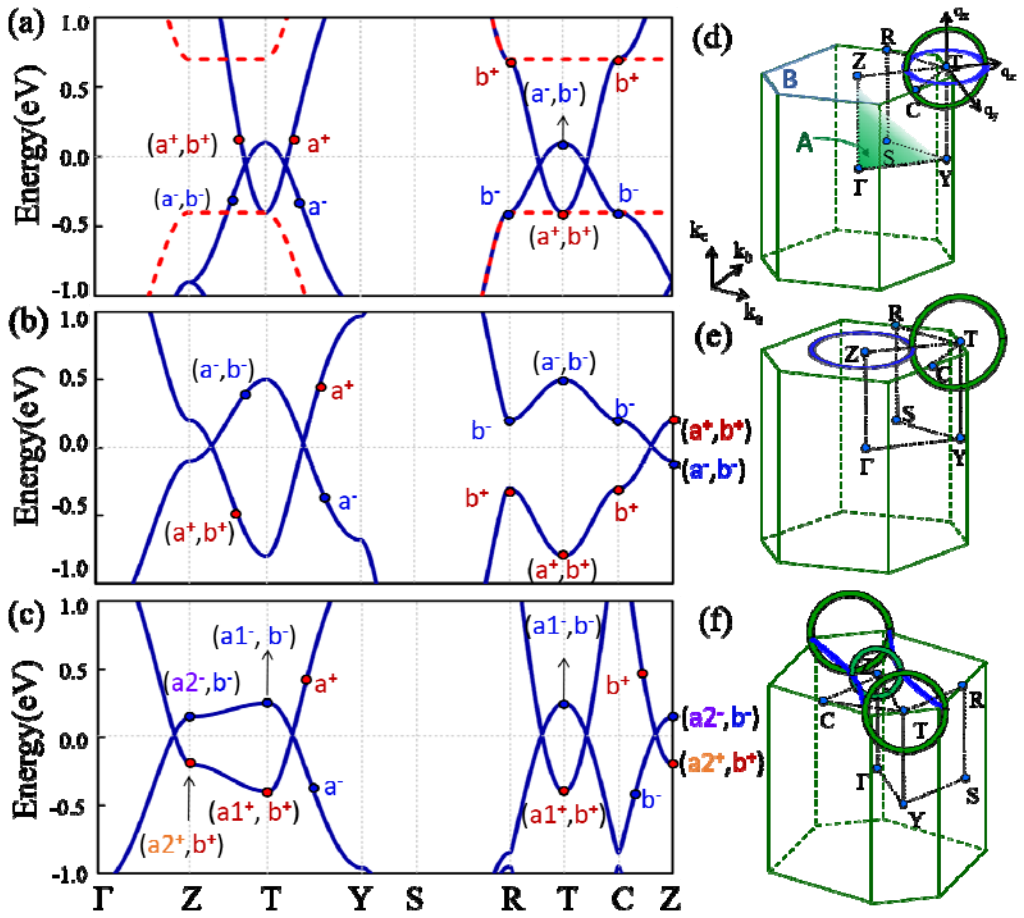


Figure 3. (color online) Band structures based on Eq. (1) with different parameters: (a) $t_1$ = -1, $t_2$ = -0.5, $t_3$ = -1.2, $t_4$ = $t_5$ = 0, $t_6$ = 0.55, $t_7$ = 0.25; (b) $t_1$ = -2.0, $t_2$ = -1.1, $t_3$ = -1.2, $t_4$ = $t_5$ = 0, $t_6$ = 0.25, $t_7$ = 0.15; (c) $t_1$ = -0.1, $t_2$ = -0.05, $t_3$ = -1.2, $t_4$ = $t_5$ = 0, $t_6$ = 1.0, $t_7$ = 0.55. Other parameters are = 1.7, = -0.9. All the values are in units of eV. Red dashed line in (a) depicts band structure for a single-layer semiconducting with the same parameters as (a) but $t_6$ = $t_7$ = 0. (d-f) Arrangements of the topological LNRs in reciprocal space corresponding to the band structures in (a-c) respectively. In (a-c), eigenvalues for A- and B-mirror planes are shown, where the two mirror planes are illustrated in (d). Note that, in (c) and (f), the convention for the special point in B-plane is changed, and A-eigenvalues at T and Z are denoted in different symbols ($a^{\pm}$ and $a2^{\pm}$ respectively).

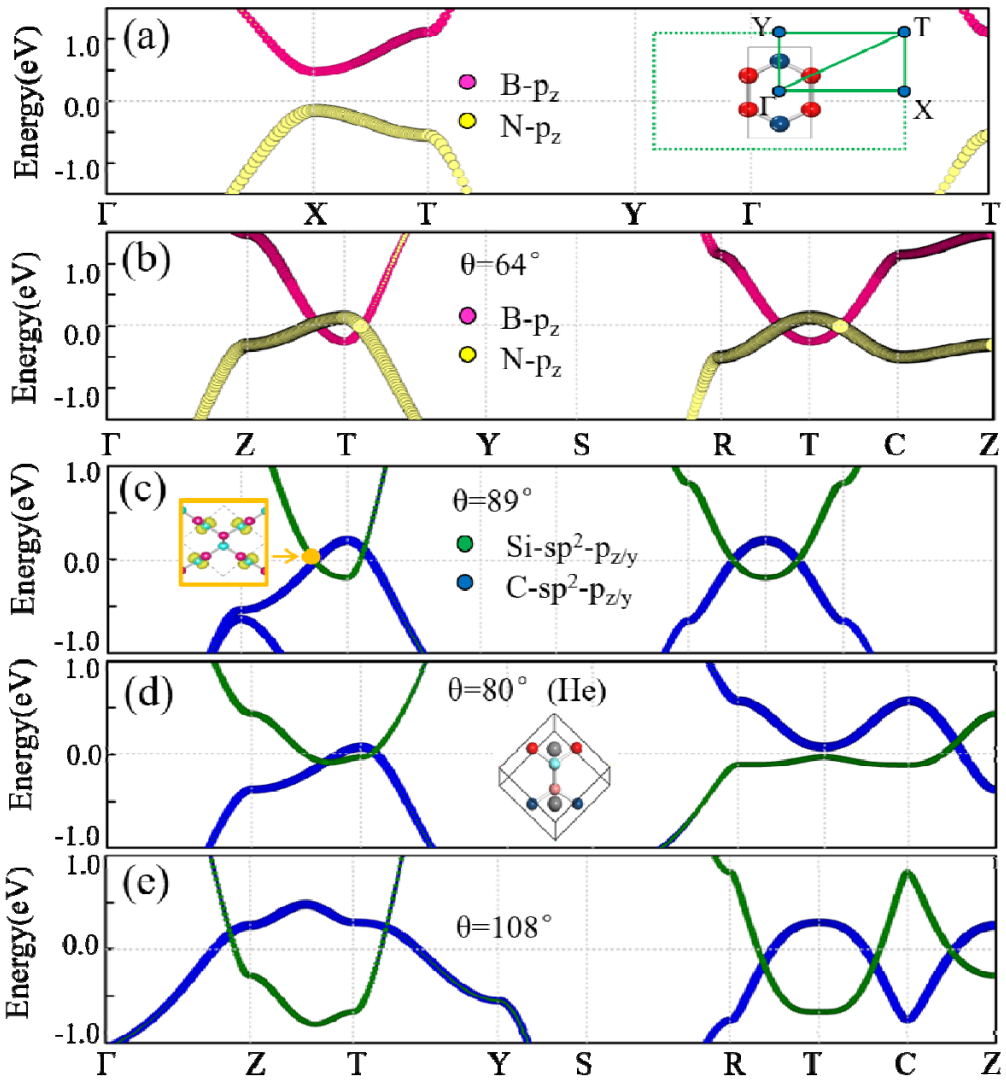


Figure 4. (color online) Projected band structures of (a) single-layer and (b) stacked 3D layered BN (see Fig. 1(a)). Projected band structures of "hidden" layered structure SiC with (c) = $89^0$, (d) = $80^0$, and (e) = $108^0$. Insets: (c) charge density of a state around the nodal point, indicating that the bonds between the atoms are similar to the bonds in graphene; (d) primitive cell of SiC with = $80^0$, where He atoms are inserted into the hole.

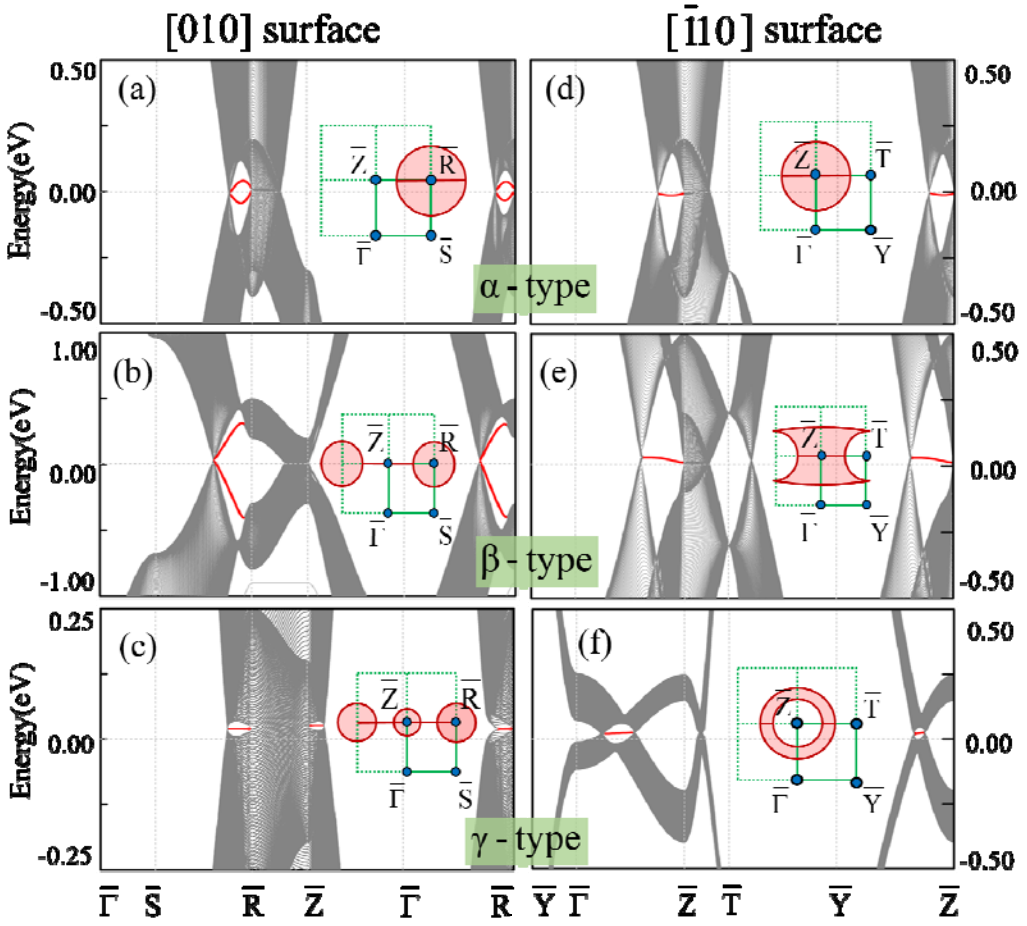


Figure 5. (color online) (a-c) Topological surface states for -, - and -type LNRs, respectively, on the [010] surface. (d-f) Same but for the [$\bar{1}$10] surface. Insets show the topological surface states regions (red shadows) in the BZ.